European Journal of Neuroscience, Vol. 25, pp. 1265–1277, 2007 doi:10.1111/j.1460-9568.2007.05356.x

The fidelity of the cortical retinotopic map in human amblyopia

Xingfeng Li,[1] Serge O. Dumoulin,[2] Behzad Mansouri[1] and Robert F. Hess[1]
[1]McGill Vision Research, Department of Ophthalmology, McGill University, Montreal, Quebec, Canada
[2]Department of Psychology, Stanford University, Stanford, California, USA

Keywords: amblyopia, cortex, fMRI, receptive field size, retinotopic mapping

Abstract

To delineate the fidelity of the functional cortical organization in humans with amblyopia, we undertook an investigation into how spatial information is mapped across the visual cortex in amblyopic observers. We assessed whether the boundaries of the visual areas controlled by the amblyopic and fellow fixing eye are in the same position, the fidelity of the retinotopic map within different cortical areas and the average receptive field size in different visual areas. The functional organization of the visual cortex was reconstructed using a fMRI phase-encoded retinotopic mapping analysis. This method sequentially stimulates each point in the visual field along the axes of a polar-coordinate system, thereby reconstructing the representation of the visual field on the cortex. We found that the cortical areas were very similar in normals and amblyopes, with only small differences in boundary positions of different visual areas between fixing and fellow amblyopic eye activation. Within these corresponding visual areas, we did find anomalies in retinotopy in some but not all amblyopes that were not simply a consequence of the poorer functional responses and affected central and peripheral field regions. Only a small increase in the average (or collective) receptive field size was found for full-field representation in amblyopes and none at all for central field representation. The former may simply be a consequence of the poorer functional responses.

Introduction

Amblyopia is a common condition (incidence 2–4%) in which the vision through one eye fails to develop due to a disruption of early visual development. Such a disruption can be due to eye-misalignment (strabismus), unequal refractive error (anisometropia) or a lack of pattern vision (form deprivation). The deficit that results is cortical in nature (Cleland *et al*., 1980; Cleland *et al*., 1982; Hess & Baker, 1984; Hess *et al*., 1985). The condition involves a reduction in the visibility of objects, quantified in terms of contrast sensitivity (Gstalder & Green, 1971; Hess & Howell, 1977; Levi & Harwerth, 1977) and inaccuracies and misperceptions of object location, quantified in terms of positional accuracy (Pugh, 1958; Hess *et al*., 1978; Bedell & Flom, 1981; Bedell & Flom, 1983; Levi & Klein, 1983; Bedell *et al*., 1985; Fronius & Sireteanu, 1989; Lagreze & Sireteanu, 1991; Fronius & Sireteanu, 1992; Hess & Holliday, 1992; Lagreze & Sireteanu, 1992b; Sireteanu *et al*., 1993a; Fronius & Sireteanu, 1994; Popple & Levi, 2005).

The neural basis of the contrast loss is thought to involve the selective loss of sensitivity of a subset of cortical cells that respond to higher spatial frequency information in the central part of the visual field (Eggers & Blakemore, 1978; Chino *et al*., 1983; Movshon *et al*., 1987; Crewther & Crewther, 1990; Kiorpes *et al*., 1998). However, virtually nothing is known about the neural basis of the deficit for the encoding of object location, which involves misperception and inaccuracy of object locations (Pugh, 1958; Hess *et al*., 1978; Bedell & Flom, 1981; Bedell & Flom, 1983; Levi & Klein, 1983; Bedell *et al*., 1985; Fronius & Sireteanu, 1989; Lagreze & Sireteanu, 1991; Fronius & Sireteanu, 1992; Hess & Holliday, 1992; Lagreze & Sireteanu, 1992b; Sireteanu *et al*., 1993a; Fronius & Sireteanu, 1994; Popple & Levi, 2005). As a similar deficit occurs in animals deprived of vision during the critical period of visual development (Gingras *et al*., 2005b), it is thought to represent a disruption of an important, albeit poorly understood, aspect of visual development.

To better understand the neural basis of this deficit for encoding the location of objects, we have set out to provide answers to some very basic questions that might bear upon how information pertaining to spatial location is represented in the visual cortex of amblyopic observers. We assume that the retinotopic organization that has been demonstrated from single cell neurophysiology (Daniel & Whitteridge, 1961), magnetic resonance imaging (Horton & Hoyt, 1991) and fMRI (Engel *et al*., 1994; Sereno *et al*., 1994; Sereno *et al*., 1995a; Engel *et al*., 1997) in various visual areas is a necessary, though not sufficient, prerequisite for accurate position coding. We use functional brain imaging (fMRI) to identify and retinotopically map visual areas to answer the following questions. (i) Are the boundaries of the retinotopically defined visual areas similar in normal and amblyopic visual systems? (ii) Is the retinotopic map within different visual areas laid out with the same fidelity in normal and amblyopic visual systems? (iii) Is the average receptive field size larger in V1 when driven by the amblyopic eye?

Materials and methods

Subjects

Eleven amblyopic subjects (average age 34 ± 15 year) were used in the study. Table 1 shows the clinical data obtained after an ophthalmological and orthoptic assessment. Clinically, amblyopia in

Correspondence: Dr Robert F. Hess, as above.
E-mail: robert.hess@mcgill.ca

Received 29 August 2006, revised 24 November 2006, accepted 12 December 2006

TABLE 1. The clinical data obtained after an ophthalmological and orthoptic assessment

Observer	Age (years) and sex	Type	Refraction	Acuity	Grating acuity	Contrast sensitivity at 1 c.p.d.	Squint, eye-movement, and eccentric fixation	History
DV	23/Female	LE mixed	+0.25 +2.75–1.25×175°	20/20 20/40	35.6 26.0	0.01 0.01	ET 3°, steady, central	Detected age 5–6 years patching for 6 months, no surgery
EF	56/Male	LE strab	+2.00+1.00×180° +2.00+1.00×130°	20/32 20/250	23.5 17.0	0.023 0.021	ET 6°, unsteady, central	Detected age 6 years, patching for 1–2 years, no surgery
GN	30/Male	RE mixed	+5.00–2.00×120° +3.50–1.00×75°	20/70 20/20	22.5 28.4	0.028 0.021	ET 8°, unsteady, 1°st	Detected age 5 years, patching for 3 months, no glasses tolerated, 2 strabismus surgery RE age 10–12 years
HP	33/Male	LE strab	−2.0+0.50 DS +0.50 DS	20/25 20/63	33.9 30.0	0.011 0.016	ET 5°, steady, central	Detected age 4 years, patching for 6 months surgery aged 5 years
LM	20/Female	RE mixed	+1.0–0.75×90° −3.25 DS	20/80 20/25	31.2 37.2	0.016 0.015	ET 6°, steady, central	Detected age 5 years, patching for 2 years
MB	50/Male	RE strab	−1.00 DS +1.00 DS	20/32 20/80	27.9 28.0	0.009 0.014	ET 3°, steady, central	No surgery, first glasses at 32 years old
MG	30/Female	RE strab	−0.50 DS +0.50 DS	20/100 20/15	20.0 52.0	0.015 0.011	ET 1°, steady, 2°n	Detected age 4 years, patching for 6 months no surgery
OA	21/Male	RE mixed	+4.50–5.00×30° −1.75−1.75×150°	20/120 20/32	18.6 33.6	0.016 0.011	ET 5°, steady, 2°n	Detected at age 3 year, Rx and patching given at 3 year, no surgery
VE	69/Male	LE mixed	−1.75–1.75×150° +4.5–5.00×30°	20/25 20/80	32.1 10.8	0.012 0.014	ET 5°, steady, central	Detected age 10 years, no treatment
XL	31/Female	RE strab	−2.75+0.75×110° −2.50 DS	20/400 20/20	11.3 31.9	0.033 0.015	ET 15°, unsteady, central	Detected age 13 years, no treatment
YC	31/Male	LE strab	+2.00 DS +2.00 DS	20/15 20/40	55.5 42.3	0.007 0.008	ET 10°, steady, central	Detected age 2 years, patching for 4 years, glasses for 16 years

LE, left eye, RE, right eye; c.p.d., cycles per degree; LE, left eye, RE, right eye; n, nasal, st, superior temporal, strab, strabismic amblyopia; DS, dioptre sphere; entries for grating acuity, contrast sensitivity, correction and fixation columns are quoted for right and left eyes, respectively.

humans can be subdivided into pure strabismus without anisometropia, pure anisometropia without strabismus and a mixed form where strabismus and anisometropia coexist. Six of our subjects had strabismic amblyopia, five had mixed strabismic/anisometropic amblyopia. During both the fMRI and psychophysics sessions, subjects wore nonmagnetic spectacles to give them corrected acuity based on refraction. A control group of six normal subjects (average age 29.8 ± 4 year) was also tested. During the scanning sessions, subjects monocularly viewed a stimulus back-projected into the bore of the scanner and viewed through an angled mirror. The eye not being stimulated was occluded with a black patch that excluded all light from the eye. All studies were performed with the informed consent of the subjects and were approved by the Montreal Neurological Institute Research Ethics Committee and in accordance with the Helsinki Declaration of human rights.

Stimuli

The stimuli in this experiment were standard retinotopic wedge and annulus checkerboard sections used for retinotopic mapping (Engel *et al.*, 1994; Sereno *et al.*, 1995b). The abruptly alternating radial square wave checkerboard had a fundamental temporal frequency of 8 Hz. The fundamental circumferential spatial frequency of the checks varied from 1.0 c.p.d. centrally to 0.1 c.p.d. peripherally. Both stimuli completed a full cycle in 60 s (TR 3; 20 × TR per cycle) with a total of six cycles per scanning run. The checkerboard had a contrast of 80%. The wedge subtended 90 degrees. The radial checkerboard contained 20 radial spokes, 10 concentric bands and subtended a visual angle of 34 degrees. The subject was instructed to attend to a central fixation point.

Stimuli were presented in a phased-encoded paradigm, always alternating runs between the left and right eyes of normal subjects or the fixing and amblyopic eyes of amblyopic subjects whilst the subject attended to a fixation spot and performed a visual task designed to control for attention. This task involved the detection of a coherent patch of checkerboard within the checkerboard stimulus as a whole that appeared at random times and positions. The responses were recorded via an optically isolated mouse to monitor the subject's attentive state. All stimuli were back-projected onto a translucent screen using a NEC 820 LCD video projector. Amblyopes (fixing as well as amblyopic eye) performed as well as normals on this task with responses well above chance but below a performance ceiling (i.e. 90–95% correct).

Using an automatic volumetric analysis (Dumoulin *et al*., 2003) that allows automatic identification of different retinotopic visual areas without the need for cortical surface reconstruction, we defined the retinotopic areas separately for each eye stimulation for normals and for our amblyopic subjects. From this we defined retinotopic areas for each subject by using the information derived from each eye separately. We defined the common retinotopic boundaries by combining the visual field sign (VFS) maps (VFS indicates whether the cortical representation of the visual field is a mirror-image or nonmirror-image reflection of the visual field) obtained from monocular stimulation to allow the comparison of the function of these common volumes of interest (VOIs) for dominant and nondominant eye stimulation of normals and for fixing and fellow amblyopic stimulation of amblyopes.

Image acquisition

A Siemens 1.5T Sonata scanner was used to collect both anatomical and functional images. Anatomical images were acquired using a head coil (circularly polarized transmit and receive) and a T1 weighted sequence (TR 22 ms; TE 10 ms; flip angle 30°) giving 180 sagittal slices of 256×256 mm^3 image voxels. Functional scans for each subject were collected using a surface coil (circularly polarized, receive only) positioned beneath the subject's occiput. Each functional imaging session was preceded by a surface coil anatomical scan (identical to the head coil anatomical sequence, except that $80 \times 256 \times 256$ sagittal images of slice thickness 2 mm were acquired) in order to later coregister the data with the head-coil image. Functional scans were multislice T2*-weighted, gradient-echo, planar images (GE-EPI, TR 3.0 s, TE 51 ms, flip angle 90°). Image volume consisted of 30 slices orthogonal to the calcarine sulcus. The field of view was 256×256 mm, the matrix size was 64×64 with a thickness of 4 mm giving voxel sizes of $4 \times 4 \times 4$ mm. Each experiment consisted of four acquisition runs for each eye (two eccentricity runs, two polar angle runs, two clockwise order, two count-clockwise) each of 128 image volumes acquired at three second intervals (TR) for either the left and right eye of normals or the fixing and amblyopic eye of amblyopes. Runs were alternated between the eyes in each case.

Data analysis

Anatomical images

The global T1 weighted aMRI scans were corrected for intensity nonuniformity (Sled *et al*., 1998) and automatically registered (Evans *et al.*, 1993) in a stereotaxic space using a stereotaxic model of 305 brains (Evans and Collins *et al*., 1994). The surface-coil aMRI, acquired in the same session as the functional images, was aligned with the head-coil aMRI, thereby allowing an alignment of the functional data with a head-coil MRI and subsequently stereotaxic space. A validation of this method was described in a previous study (Dumoulin *et al*., 2000). aMRIs were classified (Zijdenbos *et al*., 2002) into grey matter, white matter, and cerebrospinal fluid (CSF), after which the four (at the white–grey and grey–CSF boundary, for the, left, and right hemisphere) cortical surfaces for all subjects were reconstructed (MacDonald *et al*., 2000; Kim *et al*., 2005; Lerch & Evans, 2005).

Functional images

Dynamic motion correction for functional image time series for each run and for different runs were realigned using an alignment algorithm (Collins *et al*., 1994) after 3D gaussian low pass filtering (FWHM 6 mm) of time series data. The first eight scans of each functional run were discarded due to start-up magnetization transients in the data. Automatic volumetric segmentation method was used to calculate the VFS map (Dumoulin *et al*., 2003). Phase and magnitude of the response fMRI time series were calculated based on fast Fourier transformation. The signal-to-noise ratio (SNR) of each voxel was calculated based on the assumption that the standard deviation of the phase error is the inverse of the SNR of the response amplitude at the stimulation frequency (Warnking *et al*., 2002). For duty cycle estimation, the BOLD response curve was fitted to the rectangular wave that was smoothed by convolution with Gaussian (FWHM 6 mm). The best fitting smoothed rectangular wave (see Appendix) was found using a least squares criterion and the duty cycle of this waveform was used as the basis of an estimate of receptive field size (Tootell *et al*., 1997; Smith *et al*., 2001).

Eye-movement measurement

The fixation eye-movements for the normal and fellow amblyopic eyes were measured monocularly for each subject outside the scanner with a Cambridge Research Systems Video Eye-Tracker which sampled fixations at 50 Hz. Eye-movements were measured in two periods each of 90-s duration. No significant difference was found between the eye-movement variability measured in the first half compared with the last half. During one period, the other eye was patched. The subject was asked to fixate on a central fixation mark similar to that used in the scanner.

Eccentric fixation

The degree of eccentric fixation was measure in all subjects using a Heine-beta visuscope and is shown in Table 1. We decentred the fixation mark on the mapping stimulus when the amblyopic eye of subjects who exhibited eccentric fixation was scanned so that the mapping stimulus was always centred on the anatomical fovea.

Eye occlusion

To test monocular function, we occluded either the fixing or fellow amblyopic eye with a black patch designed to exclude all light. This was performed for both the psychophysical testing and for the brain imaging. Under these conditions there is no binocularly mediated suppression of the amblyopic eye as all pattern vision in the good eye has been abolished (Harrad & Hess, 1992) and thus our estimates of the reduced activation in the brains of amblyopes is a conservative one as it does not include a binocular suppressive component.

Eye dominance

We used the traditional sighting test to establish dominance (Rosenbach, 1903).

Results

Visual field sign maps

In Fig. 1 we show an illustration of the boundaries of the various retinotopic visual areas as measured by fixing and fellow amblyopic eye stimulation compared with the combined field sign boundaries (yellow/blue regions) for two amblyopic subjects. We found good agreement (black lines) between the boundaries of fixing and fellow amblyopic eye activation in our sample of strabismic amblyopes (see examples in Fig. 1, the greater the boundary difference, the more red dotted lines). A small degree of variation (indicated by red dotted lines) was detected when the between-eye boundary (within a template that included identified retinotopic visual areas) correlations for

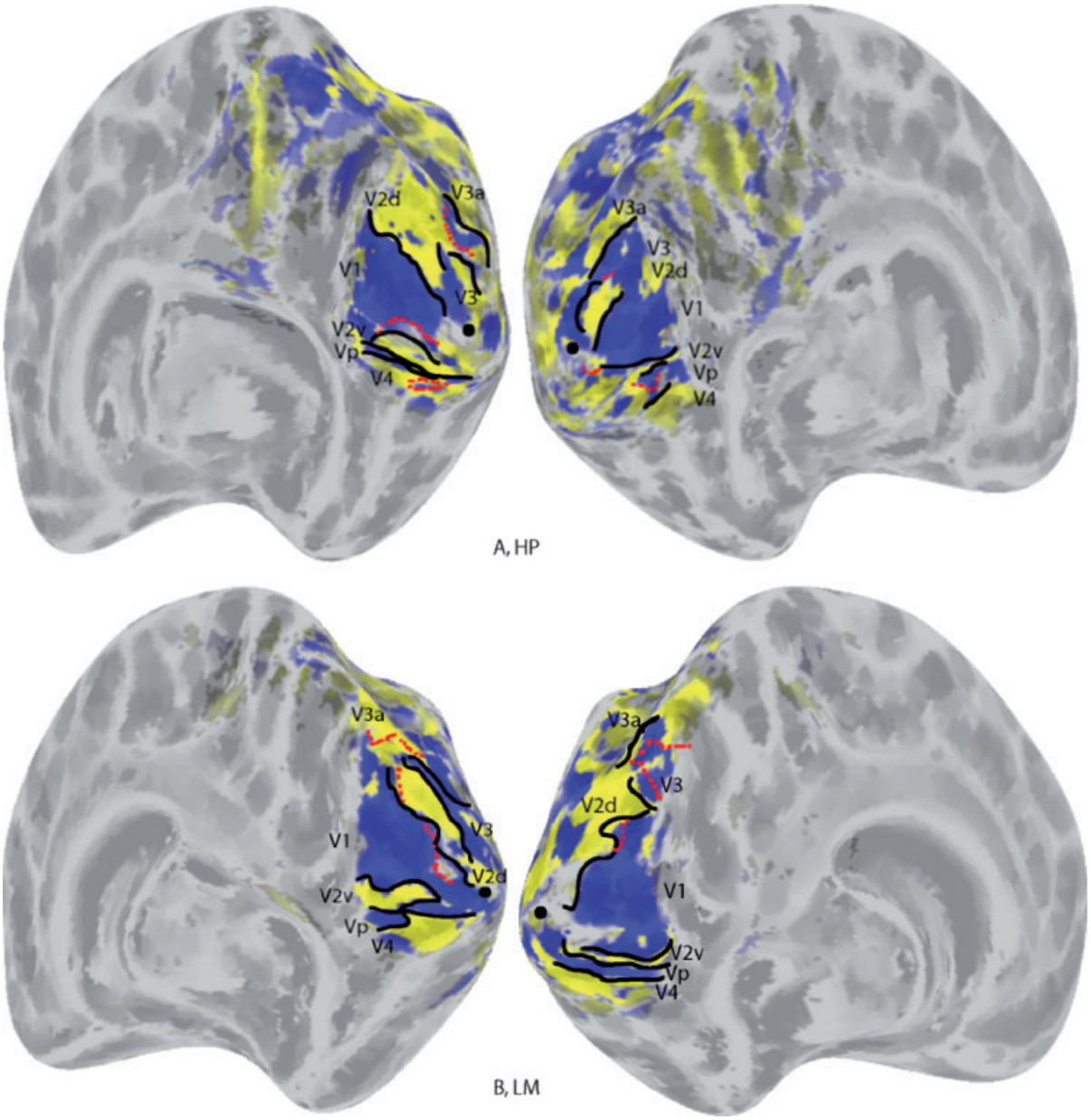

FIG. 1. Boundaries of the retinotopic visual areas for two amblyopes displayed on inflated cortex. Comparison of the boundaries for fixing and fellow amblyopic eye stimulation with the combined field sign boundaries (yellow/blue regions; VFS map calculated from averaging fixing and amblyopic eye data to the same stimuli). If the boundaries for the two eyes are the same then only the solid black lines are visible. The red dotted lines indicate when the boundaries for the amblyopic eye differ from that of the fellow fixing eye.

amblyopes were compared with the between-eye boundary correlations of normal subjects.

The results shown in Fig. 2 explores one possible reason for this small difference in the boundaries of the different retinotopic areas for amblyopes and normals, namely that it is simply a consequence of the reduced SNR responses obtained from amblyopic eye activation. As there was no consistent rule to where these differences in the visual area boundaries occurred we derived an overall similarity measure using correlational analysis for each subject. These between-eye cross-correlations for normals and amblyopes are plotted against the SNR measure of their respective responses to test this idea. Two things are evident; (i) on average, amblyopes, compared with normals, exhibit significantly lower correlations ($t = 3.661$; d.f. $= 15$; $P < 0.05$) between the VFS maps obtained from fixing and fellow amblyopic eyes and response magnitudes have significantly reduced SNR ($t = 3.744$; d.f. $= 15$; $P < 0.05$); (ii) there is no significant correlation ($r = 0.46$; NS; $p > 0.05$) between the reduced signal-to-noise response associated with the activation of the amblyopic visual system (i.e. SNR difference between eyes) and the variability of the boundaries of the visual areas (i.e. VFS correlation and reduced SNR associated with amblyopic activation), suggesting that the former is not merely a side-effect of the latter.

Retinotopy

In order to assess the fidelity of the retinotopic maps within any of the visual areas, we compared the scatter in the phase responses for the

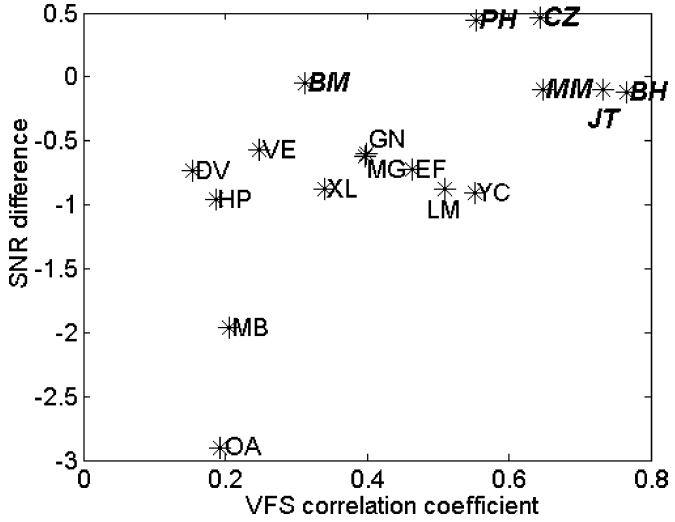

FIG. 2. Individual results are shown for normals (initials bolded) and amblyopes (initials unbolded) of the VFS correlations plotted against the corresponding SNR of the magnitude responses. Neither group exhibits a significant correlation between these two measures.

polar angle and eccentricity stimuli between eyes. We interpret any scatter in the response phase to stimuli varying in either polar angle or eccentricity as an indication of increased variability in the retinotopy of the visual map within a particular area.

In Fig. 3, by way of example we plot the V1 phase responses in radians just for the polar angle stimulus (two runs) for fixing eye activation vs. amblyopic eye activation for three amblyopes (Fig. 3A, C and E) and compare these with similar between-eye response comparisons for three normal observers (Fig. 3B, D and F). Comparing normals with amblyopes, amblyopes display more scatter between the phase responses for fixing vs. amblyopic eye activation across the visual field. We quantified this by the variance of the phase response for between-eye stimulation. Three points are noteworthy. First, there are significantly greater phase discrepancies in two (i.e. HP & OA) out of the three amblyopes shown here (Fig. 3A, C and E; EF, $t = 0.051$, d.f. $= 454$; NS; HP, $t = 2.263$, d.f. $= 530$, $P < 0.05$; OA, $t = 2.205$, d.f. $= 608$, $P < 0.05$) compared between eyes (Fig. 3B, D and F). Second, reduction in the magnitude response and an increased scatter in the phase response do not go hand in hand (e.g. EF exhibited the greatest reduction in magnitude compared with HP or OA but no significant phase scatter), suggesting these two response measures are not dependent on one another, at least over the range found for our amblyopic sample. Third, amblyopes with only moderate acuity loss (e.g. HP) can exhibit more scatter in their phase maps and amblyopes with severe acuity loss (e.g. EF) can exhibit near normal phase correspondence. In general, in our sample of amblyopes we did not find a significant correlation ($r = 0.2$; NS; $p > 0.05$) between the phase scatter and the visual acuity of the amblyopic eye.

At this stage we can only say that there is an interocular problem, it being indeterminate whether it is due to an anomaly associated with activation of the amblyopic eye, the fixing eye or both.

Figure 4 shows the group differences in the phase variance measure for normals (comparing dominant with nondominant) and amblyopes (comparing fixing with amblyopic). This comparison of responses for each eye activation allows us to show that the increased interocular phase variance illustrated in Fig. 3 is due to amblyopic eye activation. For this analysis we use both the polar angle and eccentricity response variance. Not all amblyopes exhibit an increase in the scatter of their between-eye phase response, out of our group of 11, we identified five who exhibited a statistically significant difference in their phase maps in one or more of the visual areas. Of these only three subjects (HP, EF & OA) exhibited increased phase scatter that was statistically significant (responses averaged across runs) in all the identified areas (i.e. V1, V2, V3, VP, V3A and V4). This intersubject variability meant that our amblyopes as a group (see Table 2) exhibited only slightly greater phase scatter in the amblyopic eye (Fig. 4), reaching significance (Table 2) in V1, V2, V3 and V4 ($P < 0.05$).

To assess whether the increased phase variance associated with amblyopic eye activation was restricted to only a region of the visual field, we used the phase-encoded data derived from the eccentricity ring stimulus to construct a circular central mask of radius 8.5° and a peripheral annular mask extending from 8.5° to 17° radius. We then used the data obtained from both the eccentricity and polar angle stimuli to compare interocular phase variance in central and peripheral parts of the visual field of V1 for the five amblyopes (i.e. OA, EF, HP, LM and XL) whose full-field data exhibited a significant V1 phase anomaly. These results are displayed in Fig. 5, plotted in the same way as for Fig. 3 but with the responses obtained from central (dots) and peripheral (crosses) field regions demarked. It is clear that the abnormal phase variance displayed by the amblyopic eyes of these subjects involves both central and peripheral areas of the visual field. Table 3 shows the results of the statistical evaluation. In only two amblyopes (XL and HP) was the subfield data statistically significant, indicating that the original phase anomaly required data from the full-field stimulation. In the two cases where there was a significant subfield effect, in one case this only involved the periphery (XL) and in the other case (HP) it involved both central and peripheral areas.

Across our sample of amblyopes, we did not find a significant correlation between the phase variance difference (fixing − amblyopic) and either the VFS correlation ($r = -0.005$; NS; $P > 0.05$) or the SNR differences (fixing − amblyopic; $r = -0.05$; NS; $P > 0.05$), suggesting that these two observed differences are not closely related and that neither is simply a side-effect of the reduced SNR associated with amblyopic activation. Amblyopes do not exhibit grossly reduced amplitude responses and so such a dependence would not be necessarily expected. Either amblyopes have reduced SNR but not so reduced to affect the phase estimates or the phase scatter is a reflection of anomalous but stable phase shifts. We cannot distinguish between these two possibilities.

Average receptive field size

Our mapping stimuli also have the potential of providing information on the average receptive field size of neurons in one functional voxel ($4 \times 4 \times 4$ mm), a technique first described by Tootell *et al*. (1997) and later exploited by Smith *et al*. (2001). In principle, the time taken for a stimulus to traverse a neuron's receptive field will depend on the receptive field size and an estimate of this can be obtained from measuring the duty cycle of the response (i.e. the temporal duration of functional activation) to a mapping stimulus that changes in eccentricity or polar angle. Using this technique, Smith *et al*. (2001) were able to show the rate at which the average (or collective) receptive field size changes as a function of eccentricity in different visual areas. In the present study, we wondered whether the average receptive field size was different for the amblyopic visual system. The present animal model of amblyopia would predict a loss of small receptive fields in the central visual field representation of V1 with the consequence of

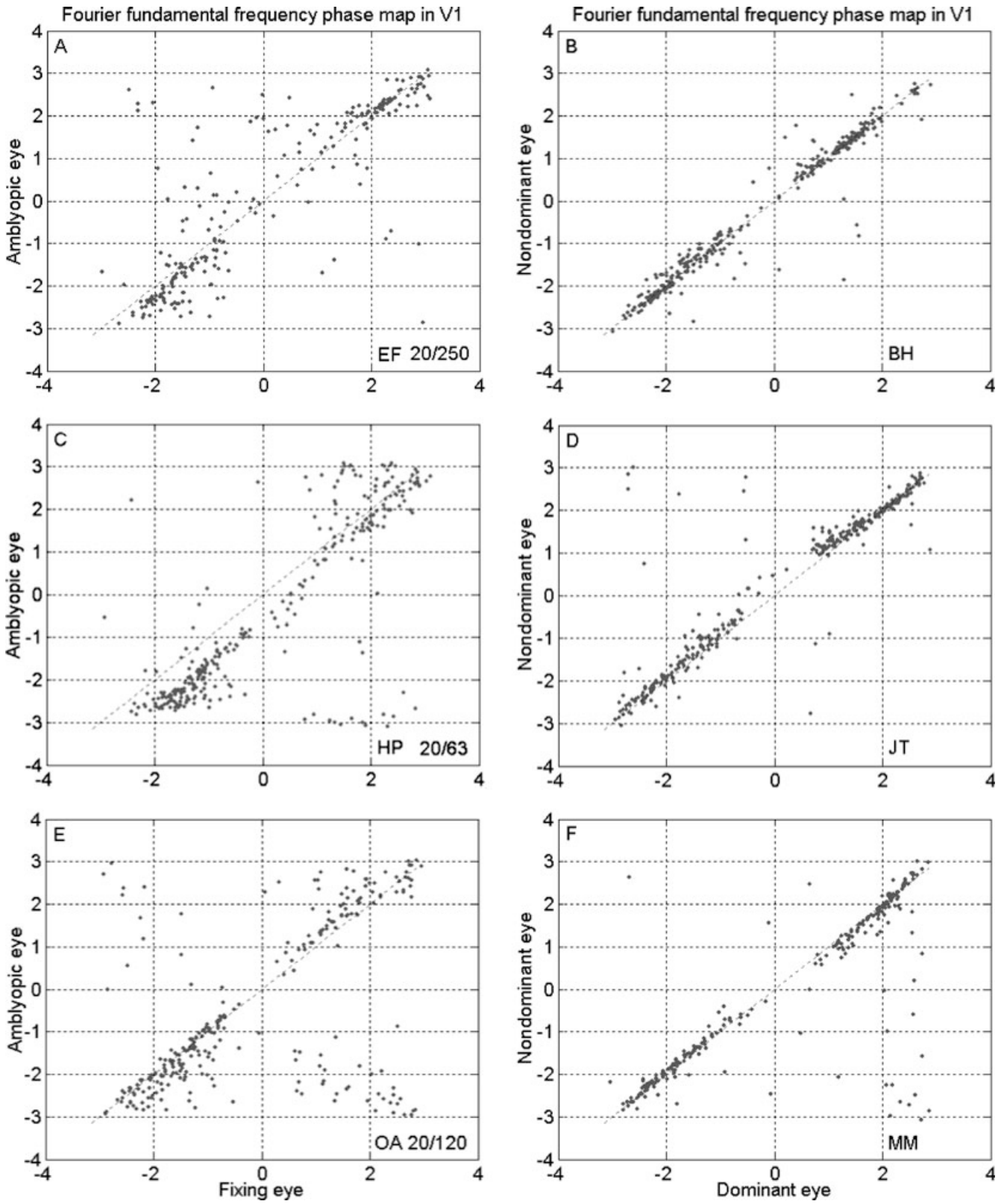

FIG. 3. Phase responses in radians (from $-\pi$ to $+\pi$) for fixing and fellow amblyopic eye stimulation are plotted against one another within area V1 defined by the averaged VFS for three representative strabismic amblyopes (A, C and E). Comparable responses are shown for three normals (B, D and F). For these subjects, amblyopic eye activation is associated with greater scatter in the phase responses.

the average receptive field size shifting to a larger value. The extent of this shift should depend on the severity of amblyopia and should strongly correlate with the acuity loss.

Figure 6 displays results from an analysis in which the duty cycle (i.e. the temporal duration of functional activation) was estimated for each eye of our normal subjects and for the fixing and amblyopic eye

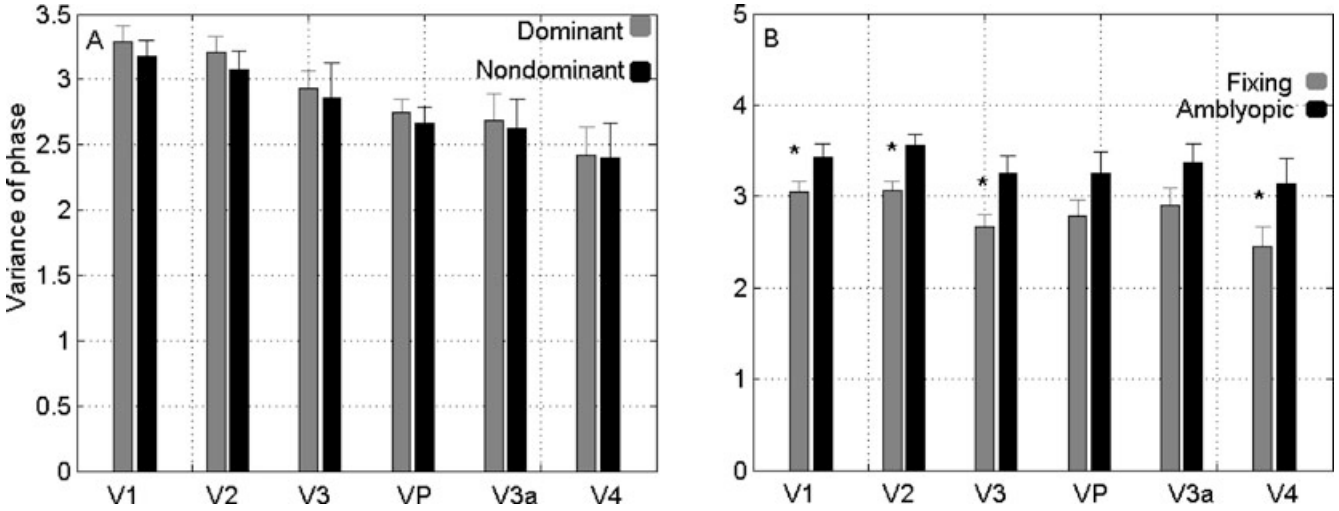

FIG. 4. Averaged phase-variance measures in the phase-encoded maps for different retinal areas in normal (A, dominant vs non-dominant) and amblyopic (B, fixing vs amblyopic) observers. On average, amblyopic activation is associated with a greater phase scatter that becomes significant in areas V1, V2, V3 and V4. *$P < 0.05$.

TABLE 2. Group comparison of phase

	t-value					
	V1	V2	V3	Vp	V3a	V4
Fixing vs. amblyopic eye	1.9958*	3.1528*	2.5636*	1.5797	1.5994	1.9679*
Fixing vs. non-dominant eye	0.6734	0.0199	0.7781	0.4658	0.8538	0.1688
Fixing vs. dominant eye	1.3062	0.8661	1.3075	0.1698	0.6860	0.1073
Dominant vs. amblyopic eye	0.5942	1.9016	1.1625	1.5416	2.0736	1.7514
Dominant vs. non-dominant eye	0.6743	0.7321	0.2293	0.4798	0. 1893	0.0680
Amblyopic vs. non-dominant eye	1.1378	2.5224*	1.2171	1.7561	2.2056*	1.7426

*$P < 0.05$ ($T > 1.96$).

of our amblyopic subjects using an eccentricity ring stimulus. For the results depicted in Fig. 6A and B, responses were averaged across the entire stimulus field of 34° diameter. There is no significant difference between the eyes of our normal controls (Fig. 6B), although we do see an increase in the average receptive field size from V1 to V4 (Smith *et al*., 2001). Our stimuli were essentially the same as those used by Smith *et al*. (2001), although our method of analysis, being in principle the same, was computationally slightly different (see Appendix). The average receptive field size was consistently larger for the amblyopic eye activation compared with the fellow fixing eye (Fig. 6A). The difference was however, small and was not significant in V1, only becoming significant in V4 (see Table 4 for summary statistics). The results for central field stimulation (Fig. 6C and D) where we would have expected to see larger differences on the basis of our current animal models (Kiorpes *et al*., 1998), indicate no differences between amblyopic vs. fixing eye stimulation.

To evaluate the finding that the slightly larger duty cycles are obtained for amblyopic stimulation using our full-field stimulus we assessed whether this increase correlated with the behavioural acuity deficit. We calculated the correlation coefficient between the difference in the duty cycle (fixing − amblyopic eye activation) for each of our individual amblyopes for area V1 and their behavoural acuity ratio (fixing/amblyopic). We found no clear relationship with the visual acuity deficit ($r = –0.078$). This is not consistent with one possibility for why our estimate of the average receptive field size in amblyopia is larger, namely that it reflects a loss of small receptive fields, as suggested by the animal models. Another explanation is that it is an artifact of the reduced SNR of the amblyopic response; more noisy activation being better fitted by response curves of slightly wider duty cycle. To assess this, we calculated the correlation coefficient between the size of the estimated duty cycle and the SNR of the response for individual subjects. The correlation was highly significant ($r = 0.92$), suggesting such a relationship.

Discussion

The functional cortical anomaly in amblyopia may not only involve a reduction in the magnitude of activation, as detailed in a number of brain imaging studies (Demer *et al*., 1988; Kabasakal *et al*., 1995; Demer, 1997; Sireteanu *et al*., 1998; Anderson *et al*., 1999; Goodyear *et al*., 2000; Barnes *et al*., 2001; Choi *et al*., 2001; Algaze *et al*., 2002; Lerner *et al*., 2003; Conner & Mendola, 2005; Muckli *et al*., 2006) but also anomalies in cortical organization. The position and size of individual retinotopic cortical areas are very similar for normals and amblyopes although there is a slightly greater degree of between-eye variation in the areal boundaries in amblyopes than normals. More importantly, there appears to be a loss of fidelity of the retinotopic map within all visual areas driven by the amblyopic eye, at least in some amblyopic subjects. These two mapping abnormalities are likely to be related as a different position estimate (phase) will yield a different border estimate because the VFS maps borders are determined by

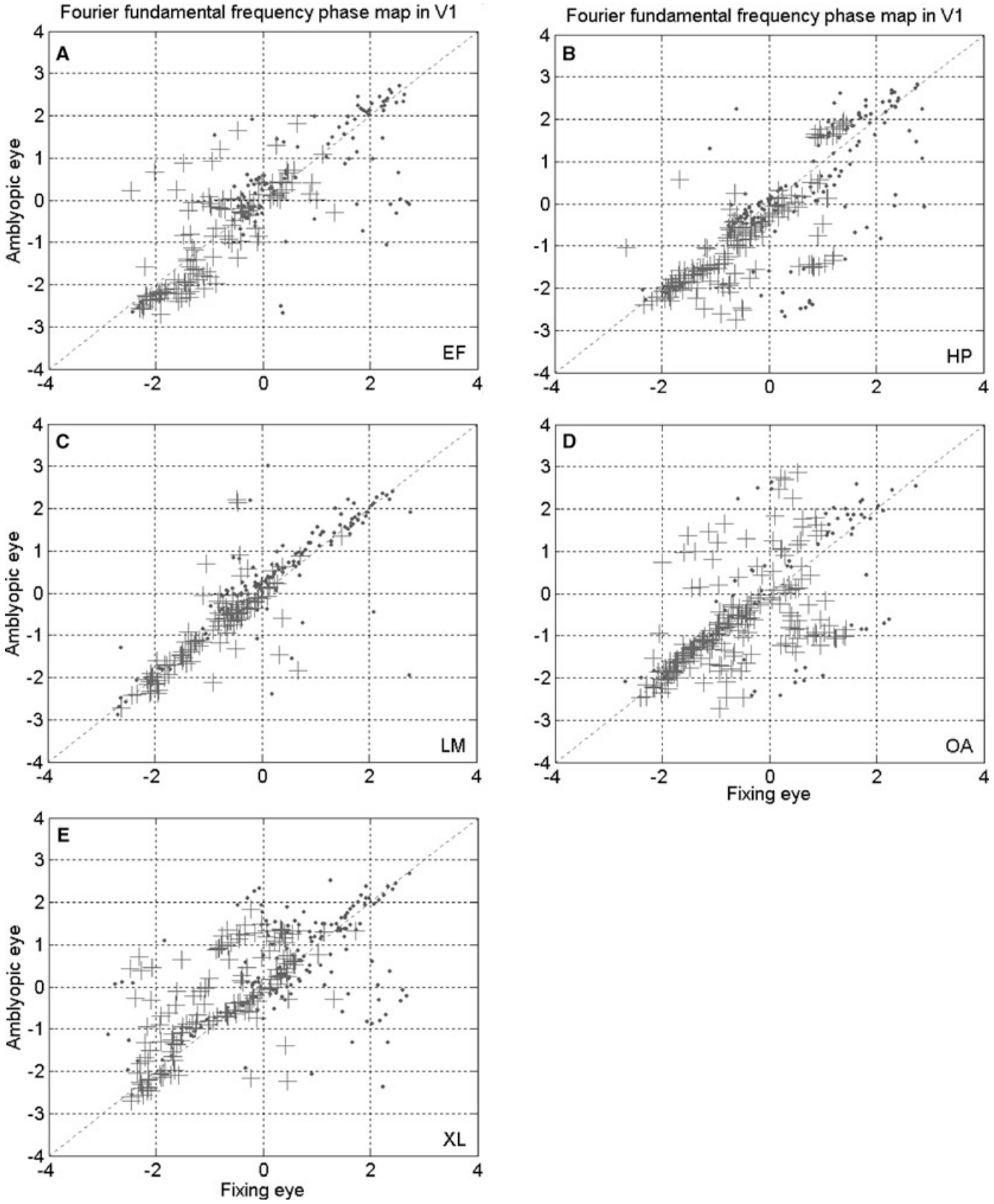

FIG. 5. Phase responses from central (8.5° radius) and peripheral (8.5° to 17°) regions are shown as dots and crosses respectively [in radians (from $-\pi$ to $+\pi$)] for fixing and fellow amblyopic eye stimulation within area V1 for the five strabismic amblyopes (A–E) who displayed anomalous phase variance for their amblyopic eye stimulation. It is clear that the phase variance anomaly involves both central and peripheral field regions and is not confined to just central vision.

TABLE 3. Phase comparison for fixing eye vs. amblyopic eye for central and for peripheral stimulation of V1 for subjects who had significantly increased phase variance for full-field stimulation of V1 of the amblyopic eye

	Central stimulation		Peripheral stimulation	
	t-value†	d.f.	*t*-value†	d.f.
EF	0.9546	226	0.1090	234
HP	2.3053*	253	3.2852*	302
LM	0.7294	234	0.4145	214
OA	0.6124	126	0.6911	402
XL	0.3729	306	3.6972*	291

*$P < 0.05$ ($T > 1.96$); d.f., degrees of freedom. †Paired *t*-test.

interpolation of neighbouring phase values (using partial derivatives of a 2D Gaussian, FWHM 3 mm, Dumoulin *et al*. 2003). There is no significant correlation between this loss of fidelity of the visual field map within visual areas driven by the amblyopic eye and either the subject's visual acuity, or the reduced SNR of the amblyopic magnitude response. Furthermore, we verified in the amblyopes who exhibited this retinotopic anomaly that it affected both central and peripheral regions of the visual field and was certainly not confined to just the central representation in V1.

We also found that the estimated average receptive field size, derived from the response duty cycle, was only slightly larger (significant only for V4 see Table 4) as a consequence of amblyopic eye activation. No significant difference in the averaged receptive field size was found between fixing and amblyopic eye activation when just the central representation of the visual field was examined. Furthermore, the difference we found for the visual field as a whole, was strongly correlated with the reduced SNR associated with amblyopic activation but not the visual acuity deficit. The most parsimonious explanation is that it may be an artifact of the poorer responses rather than reflecting genuine loss of neurons with smaller receptive fields (that only involve the central field representation) driven by the amblyopic eye. It remains a possibility that the smallest receptive fields within the central regions were not assessed because of the

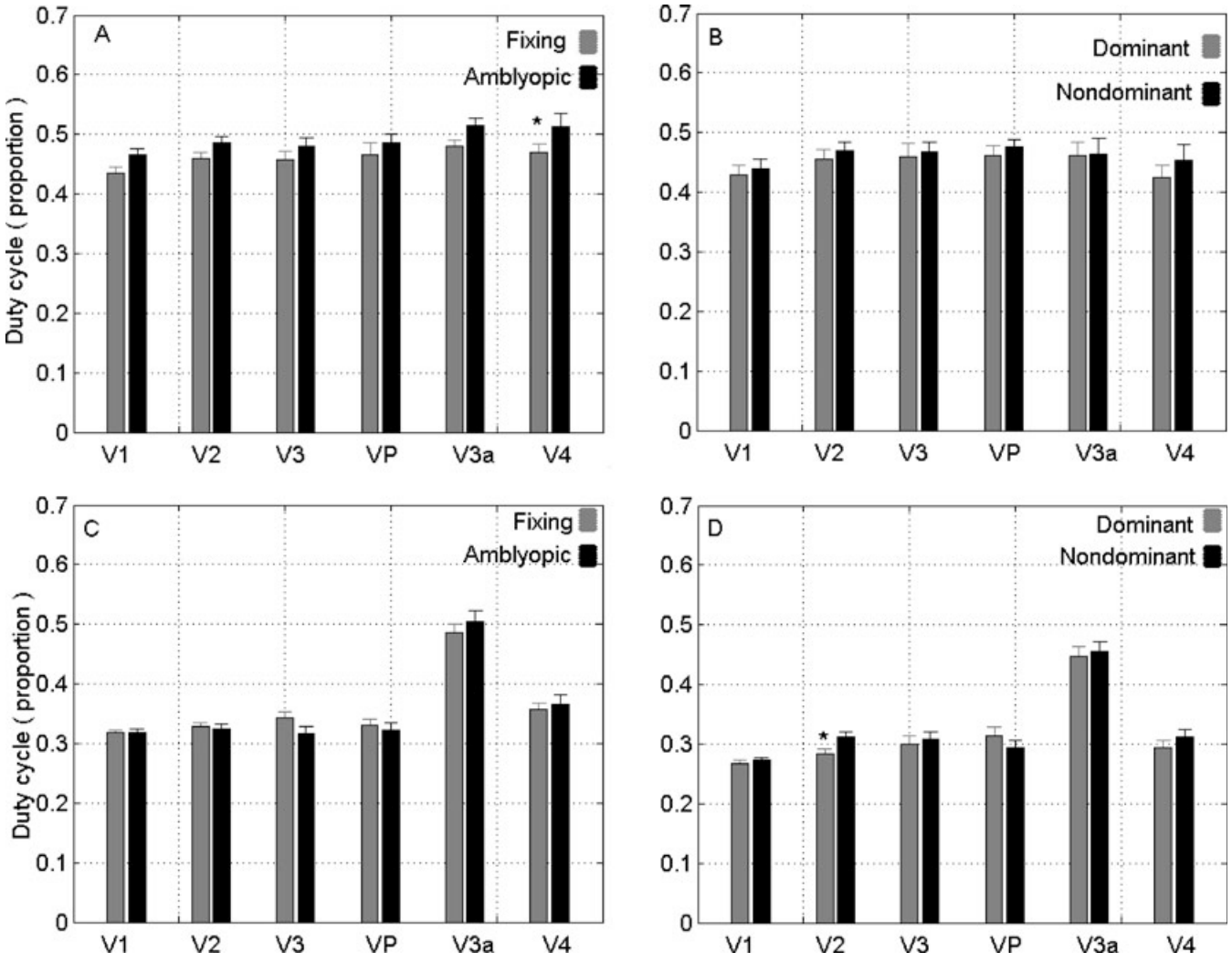

FIG. 6. The averaged duty cycle in proportional terms (i.e. temporal duration of functional activation) is given for activation of normal (dominant vs non-dominant) and amblyopic (fixing vs amblyopic) observers. In A and B, results are averaged across the visual field (34° diameter) whereas in C and D results are given for just the central visual field (17° diameter). In normals, extra-striate activation is associated with larger duty cycles. In amblyopes, the duty cycle associated with full-field amblyopic eye activation is consistently larger than that associated with fixing eye activation, this only reached significance in V4. However, the duty cycle associated with central field activation (17° diameter) is not significantly different in the amblyopic eye. *$P < 0.05$.

TABLE 4. Multiple pair *t*-test results for duty cycle

	t-value						
	d.f.	V1	V2	V3	Vp	V3a	V4
Dominant vs. non-dominant eye	10	0.424	0.649	0.316	0.620	0.063	0.859
Dominant vs. fixing eye	15	0.422	0.124	0.033	0.263	0.729	2.569*
Dominant vs. amblyopic eye	15	1.665	1.364	1.113	1.965	2.061	3.147*
Non-dominant vs. fixing eye	15	0.104	0.710	0.366	0.197	0.583	0.968
Non-dominant vs. amblyopic eye	15	1.167	0.648	0.836	1.221	1.841	2.056
Fixing vs. amblyopic eye	20	1.594	1.623	1.399	1.159	1.963	2.043*

*$P < 0.05$ ($T > 1.96$); d.f., degrees of freedom.

resolution of our analysis (voxels 4 × 4 × 4 mm). Also, as pointed out by Smith *et al*. (2001), the interpretation of this type of analysis is not straightforward. For example, average receptive field size and average receptive field scatter are confounded and influences beyond the classical receptive field may have an influence.

There are a number of possible explanations for the retinotopic mapping anomaly found in this study for some amblyopes; (i) it could be simply a side-effect of the poorer amblyopic response; (ii) it could be due to oculomotor instability of the amblyopic eye; (iii) it could result from a temporal instability in amblyopic activation, or (iv) it could reflect a loss of fidelity in the cortical map associated with the amblyopic eye. The first and most obvious explanation seems unlikely to be the sole explanation because we did not find a significant correlation between the mapping anomaly (i.e. the increased phase scatter) and the reduced SNR associated with activation of the amblyopic eye. Although one would expect some dependence between phase uncertainty and SNR in the extreme (Warnking *et al*., 2002), the lack of such a correlation in our data is not surprising owing to the relatively high SNR associated with stimulation of the amblyopic eye. The second explanation, which involves oculomotor instability, also seems unlikely. First, it has been shown previously that eye-movements less than 3° have little effect on phase-encoded fMRI responses (Baseler *et al*., 2002; Hoffmann *et al*., 2003) and none of our amblyopes had eye-movements larger than 1.8°. Secondly, it is known that the magnitude of the eye-movement abnormality in amblyopia is highly correlated (i.e. 14 min of arc of extra saccadic amplitude for every 10% change in Snell–Sterling visual acuity efficiency) with the visual acuity (Schor, 1973; Hess, 1976) yet the mapping anomaly does not correlate with the severity of the condition ($r = 0.4$; NS; $P > 0.05$). Thirdly, no significant correlation ($r = 0.4$; NS; $P > 0.05$) was found between the eye-movement deficit (ratio of average saccadic amplitudes for normal and fellow amblyopic eyes during fixation) and the phase variance deficit (ratio of phase scatter for normal and fellow amblyopic eyes). Finally, any eye-movement artifacts would be maximal for central vision where receptive fields are smallest, yet we show that the central field does not make a dominant contribution to the phase variance anomaly. As there is a time/space trade-off in the mapping paradigm, any temporal instability would result in increased phase variance. This remains an alternate explanation to that presented below in terms of the fidelity of the cortical spatial map. However, as we did not find an increased variance in the duty cycle (a measure of the temporal duration of activation) associated with amblyopic eye activation (compare the error bars in Fig. 6 for fixing, normal and amblyopic activation), we found no support for this alternate explanation.

Finally, the positional deficit in amblyopia could be due to a disarray in the visual field map in different cortical areas when driven by the amblyopic eye. A number of psychophysical investigations have revealed significant positional coding anomalies associated with amblyopic eye stimulation that might have their basis in the lack of fidelity of intra-area cortical maps. The present results showing an increase in the phase variance within the amblyopic visual system do not allow us to choose between two alternative explanations; stable but mismatched phases vs. more variable phases. The former would be relevant to mislocation errors reported in amblopia whereas the latter would be relevant to the increased positional uncertainty of amblyopic eyes. Strabismic amblyopes frequently mislocated positions within the visual field of the amblyopic eye (Bedell & Flom, 1981; Bedell & Flom, 1983; Bedell *et al*., 1985; Fronius & Sireteanu, 1989; Lagreze & Sireteanu, 1991; Fronius & Sireteanu, 1992; Lagreze & Sireteanu, 1992a; Sireteanu *et al*., 1993a; Fronius & Sireteanu, 1994; Fronius *et al*., 2000; Fronius *et al*., 2004; Popple & Levi, 2005), there is increased uncertainty about object positions within the amblyopic visual field (Levi & Klein, 1982; Levi & Klein, 1983; Levi *et al*., 1987; Hess & Holliday, 1992; Sireteanu *et al*., 1993b; Demanins & Hess, 1996) and global spatial distortions are often perceived. At present we do not know whether these different anomalies of spatial position have a common underlying neural substrate.

Traditionally, different approaches and stimuli have been used to assess the position sense in amblyopia; vernier acuity, relative position and visual field mapping. It is possible that each has its own neural substrate. At the most local level, it has been shown that there is increased uncertainty for abutting vernier stimuli especially in central parts of the field (Levi & Klein, 1982; Levi & Klein, 1983; Levi *et al*., 1987). This measure is likely to reflect neuronal filtering operations (Whitaker & MacVeigh, 1991; Wilson, 1991; Wilson & Kim, 1994) and be ultimately limited by contrast sensitivity (Carney & Klein, 1999). Such a deficit is not likely to be explained by the mapping irregularities reported here because, among other things, one would expect a strong correlation with the acuity deficit (Levi & Klein, 1982; McKee *et al*., 2003). Another approach has involved the measurement of relative spatial position by using local but not abutting reference elements (Hess & Holliday, 1992; Demanins & Hess, 1996; Popple & Levi, 2005). In this case, the positional anomaly is unrelated to the visibility defect, exhibits scale invariance and how it is distributed across eccentricity depends on spatial scale; more evenly distributed across eccentricity at the fine than the coarse scale (Demanins & Hess, 1996). This has all the hallmarks of an anomaly of position coding *per se* and because it is uncorrelated with the severity of the condition as measured with acuity, it may potentially relate to the present mapping results. At the more global level of the visual field as a whole, both perceptual and motor (i.e. pointing) approaches have been adopted to show mislocation and uncertainty of spatial position in strabismic amblyopes for reference elements placed many degrees or tens of degrees apart (Bedell & Flom, 1981; Bedell & Flom, 1983; Bedell *et al*., 1985; Fronius & Sireteanu, 1989; Lagreze & Sireteanu, 1991; Fronius & Sireteanu, 1992; Lagreze & Sireteanu, 1992a; Sireteanu *et al*., 1993a; Fronius & Sireteanu, 1994; Fronius *et al*., 2000; Fronius *et al*., 2004). These anomalies are not exclusively confined to central parts of the visual field (Demanins & Hess, 1996) and appear to be unrelated to the monocular or binocular oculomotor status of the subject (Fronius & Sireteanu, 1994). This disturbance may also potentially relate to the mapping anomalies reported here.

Finally, a possibly related spatial anomaly in amblyopia, that of perceived distortion also involves mislocation of object features within

an image. These perceptual spatial distortions are mainly reported by strabismic amblyopes and vary with spatial frequency and visual field position (Hess *et al*., 1978; Barrett *et al*., 2003). They are more exaggerated at higher spatial frequencies in more centrally located regions of the field. Their relationship to the position coding problems described above is unclear. Two different explanations have been advanced, one involving a disarray in the map topography (Hess *et al*., 1990; Hess & Field, 1994) and another involving anomalous interactions in the orientation domain (Barrett *et al*., 2003).

At present we do not know the interrelationships between these three distinct disruptions to the encoding of spatial information in amblyopia, let alone their underlying neural bases. The current animal models that are structured on the amplitude response properties of single cortical cells (Kiorpes & McKee, 1999) are unable to guide us here. However, we do know that a similar position coding behavioural deficit occurs in cats deprived of vision in early life either by strabismus or lid suture (Gingras *et al*., 2005a, b). The behavioural deficit in this case is very similar to that of human strabismic amblyopes, it involves mislocation of relative position, scale-invariance and is unrelated to the visibility disorder. In one of the few neurophysiological investigations of this issue Sireteanu & Best (1992) showed that neurons within the cat lateral suprasylvian cortex driven by the deprived eye exhibited a shift in their spatial coordinates. Recently it has been shown in two MRI studies that there may be cortical structural anomalies in humans with strabismic amblyopia (Chan *et al*., 2004; Mendola *et al*., 2005). We have recently assessed the extent to which such structural anomalies revealed by voxel-based morphometry correlate with functional anomalies in strabismic amblyopia revealed by functional MRI but have found no significant correlation (G.R. Barnes, S.D. Dumoulin, X. L. Li and R.H. Hess unpublished observations). It remains a possibility that though there is no correlation between the structure and function in terms of the decreased magnitude response, there may be one in terms of the increased scatter of the phase response.

Until we know more about how spatial position is encoded by the normal visual system it is premature to suggest that one or other of the disorders for position encoding in strabismic amblyopia described above could simply be due to a lack of fidelity of the topographic map in different cortical areas. For example, the little we do know about normal position encoding, for close but not abutting reference elements, suggests the contribution of high-level, cognitive mechanisms (Hess *et al*., 2003) and it might be at this higher cortical level that the position deficits are located in amblyopia. Finally, the abnormalities reported here were measured under monocular conditions (other eye patched) and say nothing about interocular suppression that is known to occur in this patient group.

Acknowledgements

The authors thank Bruce Hansen for testing the eye movement of the amblyopic subjects. This work was supported by a CIHR grant (MOP53346) to RFH.

Abbreviations

SNR, signal-to-noise ratio; VFS, visual field sign.

References

Algaze, A., Roberts, C., Leguire, L., Schmalbrock, P. & Rogers, G. (2002) Functional magnetic resonance imaging as a tool for investigating amblyopia in the human cortex: a pilot study. *J. AAPOPS*, **6**, 300–308.

Anderson, S.A., Holliday, I.E. & Harding, G.F. (1999) Assessment of cortical dysfunction in human strabismic amblyopia using magnetoencephalography. *Vis. Res.*, **39**, 1723–1738.

Barnes, G.R., Hess, R.F., Dumoulin, S.O., Achtman, R.L. & Pike, G.B. (2001) The cortical deficit in humans with strabismic amblyopia. *J. Physiol. (Lond.)*, **533**, 281–297.

Barrett, B.T., Pacey, I.E., Bradley, A., Thibos, L.N. & Morrill, P. (2003) Nonveridical visual perception in human amblyopia. *Invest. Ophthalmol. Vis. Sci.*, **44**, 1555–1567.

Baseler, H.A., Brewer, A.A., Sharpe, L.T., Morland, A.B., Jagle, H. & Wandell, B.A. (2002) Reorganization of human cortical maps caused by inherited photoreceptor abnormalities. *Nature Neurosci.*, **5**, 364–370.

Bedell, H.D. & Flom, M.C. (1981) Monocular spatial distortion in strabismic amblyopia. *Invest. Ophthalmol. Visual Sci.*, **20**, 263–268.

Bedell, H.E. & Flom, M.C. (1983) Normal and abnormal space perception. *Am. J. Optometry Physiol. Optics*, **60**, 426–435.

Bedell, H.E., Flom, M.C. & Barbeito, R. (1985) Spatial aberrations and acuity in strabismus and amblyopia. *Invest. Ophthalmol. Visual Sci.*, **26**, 909–916.

Carney, T. & Klein, S.A. (1999) Optimal spatial localization is limited by contrast sensitivity. *Vis. Res.*, **39**, 503–511.

Chan, S.T., Tang, K.W., Lam, K.C., Chan, L.K., Mendola, J.D. & Kwong, K.K. (2004) Neuroanatomy of adult strabismus: a voxel-based morphometric analysis of magnetic resonance structural scans. *Neuroimage*, **22**, 986–994.

Chino, Y.M., Shansky, M.S., Jankowski, W.L. & Banser, F.A. (1983) Effects of rearing kittens with convergent strabismus on development of receptive-field properties in striate cortex neurons. *J. Neurophysiol.*, **50**, 265–286.

Choi, M.Y., Lee, K.M., Hwang, J.M., Choi, D.G., Lee, D.S., Park, K.H. & Yu Y.S. (2001) Comparison between anisometropic and strabismic amblyopia using functional magnetic resonance imaging. *Br. J. Ophthalmol.*, **85**, 1052–1056.

Cleland, B.G., Crewther, D.P., Crewther, S.G. & Mitchell, D.E.M. (1982) Normality of spatial resolution of retinal ganglion cells in cats with strabismic amblyopia. *J. Physiol. (Lond.)*, **326**, 235–249.

Cleland, B.G., Mitchell, D.E.M., Gillard-Crewther, S. & Crewther, D.P. (1980) Visual resolution of ganglion cells in monocularly-deprived cats. *Brain Res.*, **192**, 261–266.

Collins, D.L., Neelin, P., Peters, T.M. & Evans, A.C. (1994) Automatic 3D intersubject registration of MR volume tric data in standardized Talairach space. *J. Comput. Assist. Tomogr.*, **18**, 192–205.

Conner, I.P. & Mendola, J.D. (2005) What does an amblyopic eye tell human visual cortex? [Abstract] *Journal of Vision*, **5**, 295a.

Crewther, D.P. & Crewther, S.G. (1990) Neural site of strabismic amblyopia in cats: spatial frequency deficit in primary cortical neurons. *Exp. Brain Res.*, **79**, 615–622.

Daniel, P.M. & Whitteridge, D. (1961) The representation of the visual field on the cerebral cortex in monkeys. *J. Physiol.*, **159**, 203–221.

Demanins, R. & Hess, R.F. (1996) Positional loss in strabismic amblyopia – interrelationship of alignment threshold, bias, spatial scale and eccentricity. *Vis. Res.*, **36**, 2771–2794.

Demer, J.L. (1997) Positron-emisson tomographic study of human amblyopia with use of defined visual stimuli. *J. AAPOPS*, **1**, 158–171.

Demer, J.L., von Noorden, G.K., Volkow, N.D. & Gould, K.L. (1988) Imaging of cerebral flow and metabolism in amblyopia by positron emission tomography. *Am. J. Ophthalmol.*, **105**, 337–347.

Dumoulin, S.O., Hoge, R.D., Achtman, R.L., Baker, C.L., Hess, R.F. & Evans, A.C. (2000) Volume tric retinotopic mapping without cortical surface reconstruction. *Neuroimage*, **11**, s613.

Dumoulin, S.O., Hoge, R.D., Baker, C.L., Hess, R.F., Achtman, R.L. & Evans, A.C. (2003) Automatic volume tric segmentation of human visual retinotopic cortex. *Neuroimage*, **18**, 576–587.

Eggers, H.M. & Blakemore, C. (1978) Physiological basis of anisometropic amblyopia. *Science (NY)*, **201**, 264–267.

Engel, S.A., Glover, G.H. & Wandell, B.A. (1997) Retinotopic organization in human visual cortex and the spatial precision of functional MRI. *Cereb. Cortex*, **7**, 181–192.

Engel, S.A., Rumelhart, D.E., Wandell, B.A., Lee, A.T., Glover, G.H., Chichilnisky, E.J. & Shadlen, M.N. (1994) fMRI of human visual cortex. *Nature*, **369**, 525.

Evans, A.C., Collins, D.L., Mills, S.R., Brown, E.D., Kelly, R.L. & Peters, T.M. (1993). *3D statistical neuroanatomical models from 305 MRI volumes*. [Proc. IEEE-Nuclear Science Symposium and Medical Imaging Conference.]

Fronius, M. & Sireteanu, R. (1989) Monocular geometry is selectively distorted in the central visual field of strabismic amblyopes. *Invest. Ophthalmol. Visual Sci.*, **30**, 2034–2044.

Fronius, M. & Sireteanu, R. (1992) Localization disorders in squint amblyopia: horizontal line bisection and relative vertical localization. *Klinische Monatsblatter Fur Augenheilkunde*, **201**, 22–29.

Fronius, M. & Sireteanu, R. (1994) Pointing errors in strabismics: complex patterns of distorted visuomotor coordination. *Vis. Res.*, **34**, 689–707.
Fronius, M., Sireteanu, R. & Zubcov, A. (2004) Deficits of spatial localization in children with strabismic amblyopia. *Graefes Arch. Clin. Exp. Ophthalmol.*, **242**, 827–839.
Fronius, M., Sireteanu, R., Zubcov, A. & Buttner, A. (2000) Preliminary report: monocular spatial localization in children with strabismic amblyopia. *Strabismus*, **8**, 243–249.
Gingras, G., Mitchell, D.E. & Hess, R.F. (2005a) Haphazard neural connections underlie the visual deficits of cats with strabismic or deprivation amblyopia. *Eur. J. Neurosci.*, **22**, 119–124.
Gingras, G., Mitchell, D.E. & Hess, R.F. (2005b) The spatial localization deficit in visually deprived kittens. *Vis. Res.*, **45**, 975–989.
Goodyear, B.G., Nicolle, D.A., Humphrey, G.K. & Menon, R.S. (2000) BOLD fMRI response of early visual areas to perceived contrast in human amblyopia. *J. Neurophysiol.*, **84**, 1907–1913.
Gstalder, R.J. & Green, D.G. (1971) Laser interferometric acuity in amblyopia. *J. Pediatric Ophthalmol.*, **8**, 251–256.
Harrad, R.A. & Hess, R.F. (1992) Binocular integration of contrast information in amblyopia. *Vis. Res.*, **32**, 135–2150.
Hess, R.F. (1976) *Threshold Contrast Sensitivity in Amblyopia*. University of Melbourne, Australia.
Hess, R.F. & Baker, C.L. (1984) Assessment of retinal function in severely amblyopic individuals. *Vis. Res.*, **24**, 1367–1376.
Hess, R.F., Baker, C.L., Verhoeve, J.N., Tulunay Keesey, U. & France, T.D. (1985) The pattern evoked electroretinogram: Its variability in normals and its relationship to amblyopia. *Invest. Ophthal. Visual Sci.*, **26**, 1610–1623.
Hess, R.F., Barnes, G., Dumoulin, S.O. & Dakin, S.C. (2003) How many positions can we perceptually encode, one or many? *Vis. Res.*, **43**, 1575–1587.
Hess, R.F., Campbell, F.W. & Greenhalgh, T. (1978) On the nature of the neural abnormality in human amblyopia; neural aberrations and neural sensitivity loss. *Pflugers Arch. – Eur. J. Physiol.*, **377**, 201–207.
Hess, R.F. & Field, D.J. (1994) Is the spatial deficit in strabismic amblyopia due to loss of cells or an uncalibrated disarray of cells? *Vis. Res.*, **34**, 3397–3406.
Hess, R.F., Field, D.J. & Watt, R.J. (1990) The puzzle of amblyopia. In Blakemore, C., (Ed), *Vision Coding and Efficiency*. Cambridge University Press, Cambridge, UK, pp. 267–280.
Hess, R.F. & Holliday, I.E. (1992) The spatial localization deficit in amblyopia. *Vis. Res.*, **32**, 1319–1339.
Hess, R.F. & Howell, E.R. (1977) The threshold contrast sensitivity function in strabismic amblyopia: Evidence for a two type classification. *Vis. Res.*, **17**, 1049–1055.
Hoffmann, M.B., Tolhurst, D.J., Moore, A.T. & Morland, A.B. (2003) Organization of the visual cortex in human albinism. *J. Neurosci.*, **23**, 8921–8930.
Horton, J.C. & Hoyt, W.F. (1991) The representation of the visual field in human striate cortex. A revision of the classic Holmes map. *Arch. Ophthalmol.*, **109**, 816–824.
Huang, N.E., Ahen, Z., Long, S.R., Wu, M.C., Ahih, H.H., Zhang, Q., Yen, N., Tung, C.C. & Liu, H.H. (1998) The empirical mode decomposition and the Hilbert spectrum for nonlinear and non-stationary time series analysis, *Proc. R. Soc. A*, **454**, 903–995.
Kabasakal, L., Devranoglu, K., Arslan, O., Erdil, T.Y., Sonmezoglu, K., Uslu, I., Tolunm, H., Isitman, A.T., Ozker, K. & Onsel, C. (1995) Brain SPECT evaluation of the visual cortex in amblyopia. *J. Nucl. Med.*, **36**, 1170–1174.
Kim, J.S., Singh, V., Lee, J.K., Lerch, J., Ad-Dab'bagh, Y., MacDonald, D., Lee, J.M., Kim, S.I. & Evans, A.C. (2005) Automated 3-D extraction and evaluation of the inner and outer cortical surfaces using a Laplacian map and partial volume effect classification. *Neuroimage*, **27**, 210–221.
Kiorpes, L., Kiper, D.C., O'Keefe, L.P., Cavanaugh, J.R. & Movshon, J.A. (1998) Neuronal correlates of amblyopia in the visual cortex of macague monkeys with experimental strabismus and anisometropia. *J. Neurosci.*, **18**, 6411–6424.
Kiorpes, L. & McKee, S.P. (1999) Neural mechanisms underlying amblyopia. *Curr. Opin. Neurobiol.*, **9**, 480–486.
Lagreze, W.D. & Sireteanu, R. (1991) Two-dimensional spatial distortions in human strabismic amblyopia. *Vis. Res.*, **31**, 1271–1288.
Lagreze, W.D. & Sireteanu, R. (1992a) Errors of monocular localization in strabismic amblyopia. Two-dimensional distortion. *Klinische Monatsblatter Fur Augenheilkunde*, **201**, 92–96.
Lagreze, W.D. & Sireteanu, R. (1992b) Errors of monocular localization in strabismic amblyopia. Two-dimensional distortion. *Klin Monatsbl Augenheilkd*, **201**, 92–96.
Lerch, J.P. & Evans, A.C. (2005) Cortical thickness analysis examined through power analysis and a population simulation. *Neuroimage*, **24**, 163–173.
Lerner, Y., Pianka, P., Azmon, B., Leiba, H., Stolovitch, C. & Loewensrein, A. (2003) Area-specific amblyopic effects in human occipitotemporal object representations. *Neuron*, **40**, 1023–1029.
Levi, M. & Harwerth, R.S. (1977) Spatio–temporal interactions in anisometropic and strabismic amblyopia. *Invest. Ophthalmol. Visual Sci.*, **16**, 90–95.
Levi, D.M. & Klein, S. (1982) Hyperacuity and amblyopia. *Nature*, **298**, 268–270.
Levi, D.M. & Klein, S.A. (1983) Spatial localization in normal and amblyopic vision. *Vis. Res.*, **23**, 1005–1017.
Levi, D.M., Klein, S.A. & Yap, Y.L. (1987) Positional uncertainty in peripheral and amblyopic vision. *Vis. Res.*, **27**, 581–597.
MacDonald, D., Kabani, N., Avis, D. & Evans, A.C. (2000) Automated 3-D Extraction of inner and outer surfaces of cerebral cortex from MRI. *Neuroimage*, **12**, 340–356.
McKee, S.P., Levi, D.M. & Movshon, J.A. (2003) The pattern of visual deficits in amblyopia. *J. Vis.*, **3**, 380–405.
Mendola, J.D., Conner, I.P., Roy, A., Chan, S.T., Schwartz, T.L., Odom, J.V. & Kwong, K.K. (2005) Voxel-based analysis of MRI detects abnormal visual cortex in children and adults with amblyopia. *Hum. Brain Mapp.*, **25**, 222–236.
Movshon, J.A., Eggers, H.M., Gizzi, M.S., Hendrickson, A.E., Kiorpes, L. & Boothe, R.G. (1987) Effects of early unilateral blur on the macaque's visual system. III. Physiological observations. *J. Neurosci.*, **7**, 1340–1351.
Muckli, L., Kiess, S., Tonhausen, N., Singer, W., Goegel, R. & Sireteanu, R. (2006) Cerebral correlates of impaired grating perception in individual psychophysically assessed human amblyopes. *Vis. Res.*, **46**, 506–526.
Popple, A.V. & Levi, D.M. (2005) Location coding by the human visual system: Multiple topological adaptations in a case of strabismic amblyopia. *Perception*, **34**, 87–107.
Pugh, M. (1958) Visual distortion in amblyopia. *Br. J. Ophthal.*, **42**, 449–460.
Rosenbach, O. (1903) Ueber monokulare Vorherrschaft beim binikularen Sehen. *Munchener Med. Wochenschriff*, **30**, 1290–1292.
Schor, C.M. (1973) *Oculomotor and Neurosensory Analysis of Amblyopia*. University of California at Berkeley.
Sereno, M.I., Dale, A.M., Reppas, J.B., Kwong, K.K., Belliveau, J.W., Brady, T.J., Rosen, B.R. & Tootell, R.B.H. (1995a) Borders of multiple visual areas in humans revealed by functional magnetic resonance imaging. *Science*, **268**, 889–893.
Sereno, M.I., Dale, A.M., Reppas, J.B., Kwong, K.K., Belliveau, J.W., Brady, T.J., Rosen, B.R. & Tootell, R.B.H. (1995b) Borders of multiple visual areas in humans revealed by functional magnetic resonance imaging. *Science*, **268**, 889–893.
Sereno, M.I., McDonald, C.T. & Allman, J.M. (1994) Analysis of retinotopic maps in extrastriate cortex. *Cereb. Cortex*, **6**, 601–620.
Sireteanu, R. & Best, J. (1992) Squint-induced modification of visual receptive fields in the lateral suprasylvian cortex of the cat: Binocular interaction, vertical effect and anomalous correspondence. *Eur. J. Neurosci.*, **4**, 235–242.
Sireteanu, R., Lagreze, W.D. & Constantinescu, D.H. (1993a) Distortions in two-dimensional visual space perception in strabismic observers. *Vis. Res.*, **33**, 677–690.
Sireteanu, R., Lagreze, W.D. & Constantinescu, D.H. (1993b) Distortions in two-dimensional visual space perception in strabismic observers. *Vis. Res.*, **33**, 677–690.
Sireteanu, R., Tonhausen, N., Mickli, L., Zanella, F.F. & Singer, W. (1998) Cortical site of amblyopic deficit in strabismic and anisometropic subjects. *Invest. Ophthal. Visual Sci. Suppl.*, **39**, s909.
Sled, J.G., Zijdenbos, A.P. & Evans, A.C. (1998). A non-parametric method for automatic correction of intensity non-uniformity in MRI data. *IEEE Trans. Med. Imag.*, **17**, 87–97.
Smith, A.T., Singh, K.D., Williams, A.L. & Greenlee, M.W. (2001) Estimating receptive field size from fMRI data in human striate and extra-striate cortex. *Cereb. Cortex*, **11**, 1182–1190.
Tootell, R.B.H., Mendola, J.D., Hadjikhani, N.K., Ledden, P.J., Liu, A.K., Reppas, J.B., Sereno, M.I. & Dale, A.M. (1997) Functional analysis of V3A and related areas in human visual cortex. *J. Neurosci.*, **15**, 7060–7078.
Warnking, J., Dojat, M., Dugue, G.A., Martin, C.D., Olympieff, S., Richard, N., Chehikian, A. & SegeBarth, C. (2002) fMRI retinotopic mapping_step by step. *Neuroimage*, **17**, 1665–1683.
Whitaker, D. & MacVeigh, D. (1991) Interaction of spatial frequency and separation in vernier acuity. *Vis. Res.*, **31**, 1205–1212.
Wilson, H.R. (1991) Model of peripheral and amblyopic hyperacuity. *Vis. Res.*, **36**, 967–982.

Wilson, H.R. & Kim, J. (1994) A model for motion coherence and transparency. *Visual Neurosci.*, **11**, 1205–1220.
Worsley, K.J., Liao, C., Aston, J., Petre, V., Duncan, G.H. & Evans, A.C., (2002). A general statistical analysis for fMRI data. *NeuroImage*, **15**, 1–15.
Zijdenbos, A.P., Forghani, R. & Evans, A.C. (2002) Automatic 'Pipeline' Analysis of 3-D MRI data for clinical trials: application to multiple sclerosis. *IEEE Transactions Med. Imaging*, **21**, 1280–1291.

Appendix

Duty cycle estimation

The time series of BOLD signal change was normalized:

$$Y(i) = \frac{S(i) - \bar{S}}{std} \tag{A1}$$

where $Y(i)$ is the normalized BOLD-fMRI time series, $S(i)$ is the raw fMRI time series, i is the sampled time point (image frame), $\bar{S}$is the mean value of the series, and *std* is the standard deviation of the time series.

Based on the general linear model (GLM; Worsley *et al*., 2002):

$$Y(i) = X\beta + \varepsilon = [X_1(i), X_2(i), \ldots, X_k(i)] \begin{bmatrix} \beta_1 \\ \beta_2 \\ \vdots \\ \beta_k \end{bmatrix} + \varepsilon \tag{A2}$$

β is the regression parameter, and ϵ is the random error, and $X(u, v)$ is the $n \times k$ design matrix. $X_1(i)$ was formed as a rectangular wave (six cycles in this study, frequency is the same as stimuli) which was smoothed by convolution with a Gaussian function (FWHM 6 mm), to simulate the BOLD response. The parameters of the rectangular were u and v. u is the onset of the rectangular (delay), and v is the width of the block. u and v are the optimized parameters in the design matrix. To eliminate the low frequency drift, we added the polynomial drift $X_2(i)$, …, $X_k(i)$ in the design matrix (we set the order of the polynomial equal to 1, $k = 3$, that is we added the $X_2(i) = 1$, and slope drift $X_3(i) = x$ in the design matrix). Least square method was adopted to solve Eqn A2.

$$\hat{\beta} = X(u, v)^{+} Y(u, v) \tag{A3}$$

$$E(u, v) = A\hat{\beta} \tag{A4}$$

Contrast matrix $A = [1\ 0\ 0]$ in this study; the estimated standard deviation is

$$S(u, v) = \|AX(u, v)^{+}\|\sigma \tag{A5}$$

where $\sigma^2 = RSS/df; df = n - rank(X(u,v))$;. The residual sum of squares RSS is calculated:

$$RSS = \left\| Y(u, v) - X(u, v)\hat{\beta} \right\|^2 \tag{A6}$$

where $\| \|$ is the norm. For each u and v, the T statistic is calculated as

$$T(u, v) = \frac{E(u, v)}{S(u, v)} \tag{A7}$$

Both delay and duty cycle were estimate using

$$u_{opt}, v_{opt} = \max(T(u, v)) \tag{A8}$$

We optimized Eqn A8 using two-dimensional full search algorithm (calculated all the cases, and use the max T-value). The best fit rectangular can be obtained

$$Y_{opt} = X(u_{opt}, v_{opt})\hat{\beta} \tag{A9}$$

After obtaining the optimization curve, we removed low drift from the design matrix using the Empirical Mode Decomposition (Huang *et al*., 1998), and subtract low drift from Y_{opt}, we obtained the drift removed optimized rectangular wave; this curve was used to calculate duty cycle, v is the width (duty cycle) and u is the delay of this response at this pixel.